Journal of the European Ceramic Society 22 (2002) 361–373

www.elsevier.com/locate/jeurceramsoc

A comparative investigation of chromium deposition at air electrodes of solid oxide fuel cells

S.P. Jiang[a,*], J.P. Zhang[b], X.G. Zheng[b]

[a]*CSIRO, Manufacturing Science and Technology, Private Bag 33, Clayton South MDC, Victoria 3169, Australia*
[b]*Ceramic Fuel Cell Limited, 170 Browns Road, Noble Park, Victoria 3174, Australia*

Received 20 October 2000; accepted 26 March 2001

Abstract

Deposition processes of chromium (Cr) species were investigated for the O_2 reduction on (La,Sr)MnO_3 (LSM), Pt and (La,Sr)(Co,Fe)O_3 (LSCF) electrodes in the presence of chromia-forming alloy metallic interconnect at 900°C under air flow. For the reaction on LSM electrodes, deposition of Cr species preferentially occurred on the zirconia electrolyte surface, forming a distinct deposit ring at the edge of the LSM electrode while at LSCF electrodes, Cr species deposited on the electrode and electrolyte surface, forming isolated Cr particles. In contrast, there was no detectable deposition of Cr species either on the electrode or electrolyte surface for the O_2 reduction reaction on Pt electrodes. The results clearly demonstrated that deposition of Cr species in solid oxide fuel cells is not an electrochemical reduction of high valent Cr vapor species to Cr_2O_3 in competition with O_2 reduction. Cr deposition at SOFC cathodes is basically a chemical dissociation reaction and is controlled by the nucleation reaction between the nucleation agent and the gaseous Cr species. The nature of the nucleation agent strongly depends on the electrode material and impurities which may be introduced during electrode and electrolyte fabrication processes.

Keywords: Electron microscopy; Fuel cells; Interconnect; (La,Sr)MnO_3; (La,Sr)(Co,Fe)O_3; Perovskites

1. Introduction

Interconnect is one of the key components in planar solid oxide fuel cells (SOFC) to connect electrically individual cells in a series to make SOFC stacks. The interconnect materials must be gas-tight, have high electric conductivity, high temperature and chemical stability, matching thermal expansion coefficient to other cell components, sufficient mechanical strength and low material and processing cost. There are two types of interconnect materials commonly used in SOFC; doped $LaCrO_3$-based ceramic materials and high temperature oxidation resistance metallic materials. Recently there has been rapid progress in the development of intermediate temperature SOFC based on thin electrolyte technology.[1–3] This greatly increases the feasibility of using low cost metallic interconnect materials.[4–7] However, high temperature oxidation resistance alloys generally contain chromium and/or aluminium as alloying additives to form a protective chromium and/or aluminium oxide scale. Thus, for a chromium-based alloy the evaporation of gaseous Cr species under oxidizing conditions is inevitable. Using dense protective coatings can substantially reduce the Cr evaporation.[8] Without effective protective coatings, the volatile Cr species can cause rapid performance deterioration of (La,Sr)MnO_3 (LSM) electrode for O_2 reduction reactions.[6,9–11] The degradation of the electrode performance is generally considered to be caused by the electrochemical deposition of Cr species at the electrode/electrolyte interface region in competition with O_2 reduction reactions.[6,9–11] The electrochemical deposition mechanism of Cr species is largely based on the thermodynamic compatibility of the negative Gibbs energy changes for the electrochemical reduction reactions of O_2 and of high valent Cr species,[9] and on the observed correlation between the intensity of Cr species deposited at the electrode/electrolyte interface region and the performance degradation for the O_2 reduction on LSM electrodes.[10] Recently, we investigated in detail the deposition processes of Cr species at LSM electrodes and the effect of Cr species on the O_2 reduction reaction under various conditions.[12–15]

* Corresponding author. Present address: School of Mechanical and Production Engineering, Nangyang Technological University, Nangyang Avenue, Singapore 639798. Tel.: +65-790-5010; fax: +65-791-1859.

E-mail address: mspjiang@ntu.edu.sg (S.P. Jiang).

0955-2219/01/$ - see front matter
PII: S0955-2219(01)00280-1

Under air flow, the deposition of Cr species occurred preferentially on the zirconia electrolyte surface under both cathodic and anodic polarization conditions. Under cathodic polarization potentials, a Cr deposit ring was formed on the zirconia electrolyte surface at the edge of the LSM electrode. In the absence of polarization, the preferential deposition of Cr species on the zirconia electrolyte surface took place for the LSM electrode heated at 1100 °C for 50 h but not at 900 °C. Without air flow, deposition of Cr species occurred on the LSM electrode surface and zirconia electrolyte surface. The deposition of Cr species on the TZ3Y electrolyte surface under the rib of the chromia-forming alloy interconnect was substantially higher than that under the channel of the interconnect. The results clearly demonstrated that Cr deposition at the LSM electrode/zirconia electrolyte system is not dominated by the electrochemical reduction of high valent Cr species in competition with O_2 reduction reactions. The driving force for the deposition of Cr species is most likely associated with Mn species in particular Mn^{2+} ions generated under polarization or at high temperatures.[13,15] Thus, it is of great scientific importance to investigate the deposition processes of Cr species at electrodes other than LSM. In this paper, the Cr deposition process is studied at Pt and (La,Sr)(Co,Fe)O_3 (LSCF) electrodes and some of the results on the LSM electrode are reproduced here for the purpose of comparison.[13,14]

2. Experimental

$La_{0.72}Sr_{0.18}MnO_3$ (LSM) and $La_{0.60}Sr_{0.40}Co_{0.2}Fe_{0.8}O_3$ (LSCF) powders were prepared by co-precipitation, followed by sintering at 1000 and 900 °C in air, respectively. Fig. 1 is the XRD patterns of LSM and LSCF powders, confirming the perovskite structure of the powder with no free lanthanum oxide. LSM electrode coating was applied to 3 mol% Y_2O_3–ZrO_2 (TZ3Y, Tosoh, Japan) electrolyte substrates by screen printing and sintered at 1150 °C for 4 h. TZ3Y electrolyte substrates were prepared by tape casting and were ca. 120 μm thick. LSCF electrode coating was applied to $Ce_{0.8}Sm_{0.2}O_2$ (SDC) electrolyte substrates by screen printing and was fired at 950 °C for 2 h in place prior to the electrochemical testing. SDC electrolyte substrates were prepared by isostatic pressing and the electrolyte thickness was ca. 900 μm. The use of SDC electrolyte in the case of LSCF electrode avoided the interfacial reaction between LSCF and zirconia electrolyte.[16] Pt electrode was prepared by slurry painting using Pt paste (Engelhard 6082). The thickness of screen-printed LSM and LSCF electrodes was ca. 50 μm and for Pt electrode it was 1–2 μm. The electrode area was 0.44 cm^2. Pt paste was painted onto the other side of the electrolyte substrates to make counter and reference electrodes. Care

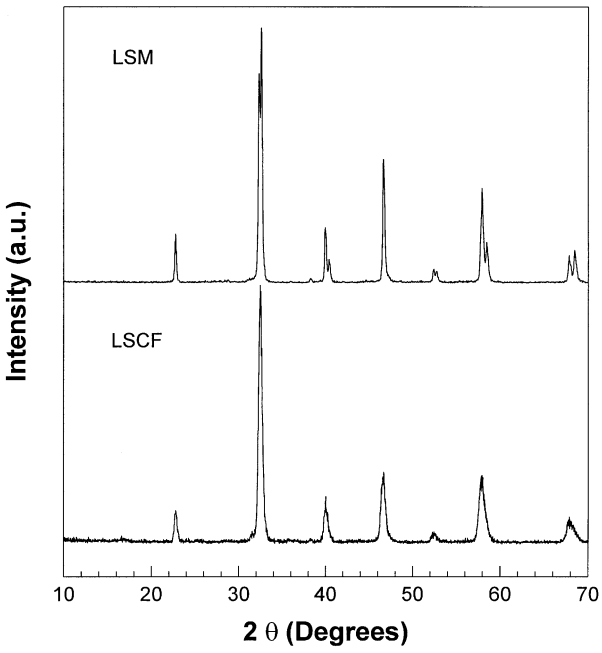

Fig. 1. XRD patterns of pre-coarsened LSM and LSCF powders.

was taken to ensure that the counter electrode was symmetrically positioned at the center opposite to the working electrode to minimize the possible error caused by the misalignment between the working and counter electrode.[17] Reference electrode was painted as a ring around the counter electrode. The gap between the counter electrode and the ring reference electrode was ca. 4 mm.

High chromium ferritic stainless steel (25 w/o Cr, 73 w/o Fe, 0.7 w/o Mn, negligible Si) was used as metallic interconnect material. The alloy was machined into coupons (12×12×5 mm thick) with channels (1.2×1.2 mm deep) cut on one side and holes in the center of each channel. Air was distributed to the electrode coating through the channel by an alumina tube. Two Pt wires were spot-welded to the coupon to serve as voltage and current probes, respectively. No Pt mesh was placed between the chromia-forming alloy interconnect and the electrode coating. In this arrangement, the chromia-forming alloy was also a current collector. Air (BOC, industrial grade, moist content $<0.01\%$) was used without further drying. The air flow rate was controlled at 100 ml min^{-1} for both working and counter electrodes. Fig. 2 shows the cell configuration and the arrangement of the chromia-forming alloy interconnect. For the experiments in the absence of chromia-forming alloy, Pt mesh was used as current collector for the working electrode. A separate sample holder was used to avoid the Cr contamination.[14]

Polarization of the electrode was carried out under a constant current density of 200 mA cm^{-2} at 900 °C in air. Cathodic polarization potential ($E_{Cathode}$) was recorded against the Pt air reference electrode using a data logging device. Polarization was interrupted from

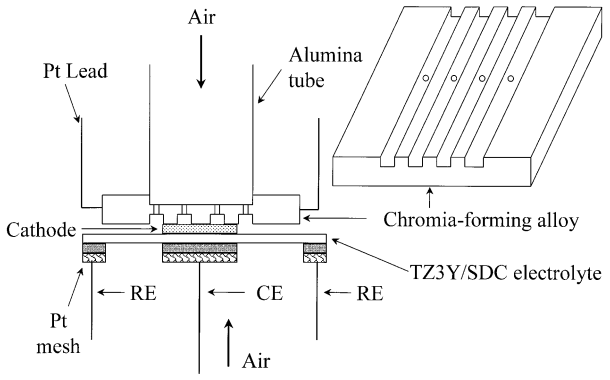

Fig. 2. Cell configuration and arrangement of the chromia-forming alloy interconnect.

time to time to measure the overpotential losses (η) and electrode ohmic resistance (R_Ω) by galvanostatic current interruption (GCI). A Leica 360 field emission scanning electron microscopy (SEM) equipped with Oxford Link energy dispersive spectroscopy (EDS) system was used to examine the electrode/electrolyte interface region and the elemental distribution of the deposits. Similar to that on the LSM electrode,[13] the deposition process of Cr species at LSCF electrodes was also studied in the absence of polarization potentials. A LSCF electrode in contact with a chromia-forming alloy interconnect coupon was heated in a tube furnace in an arrangement similar to the cell testing configuration at 900 °C for 140 h with no current passing through the cell. Air was flowing through the electrode during the heat treatment. After the heating treatment, LSCF electrode was examined by SEM and EDS.

3. Results and discussion

3.1. Electrode behavior

Fig. 3 shows the initial polarization curves of LSM, Pt and LSCF electrodes for O_2 reduction under a cathodic current density of 200 mA cm^{-2} at 900 °C in the absence of chromia-forming alloy interconnect. For O_2 reduction on LSM electrodes, the polarization potential ($E_{Cathode}$) initially started at a very high value but decreased very rapidly with the current passage. Despite the significant change in $E_{Cathode}$, the electrode ohmic resistance (R_Ω) remained more or less constant, indicating that the reduction in $E_{Cathode}$ was purely due to the reduction in η. The rapid reduction in the polarization potential for the O_2 reduction on the LSM electrode with cathodic current passage is consistent with the observed activation effect of the cathodic current/polarization on the initial LSM electrode performance.[18,19]

Pt electrode showed initially high electrochemical activity for the O_2 reduction as indicated by the initial low polarization losses ($\eta = 8$ mV at 200 mA cm^{-2} before the

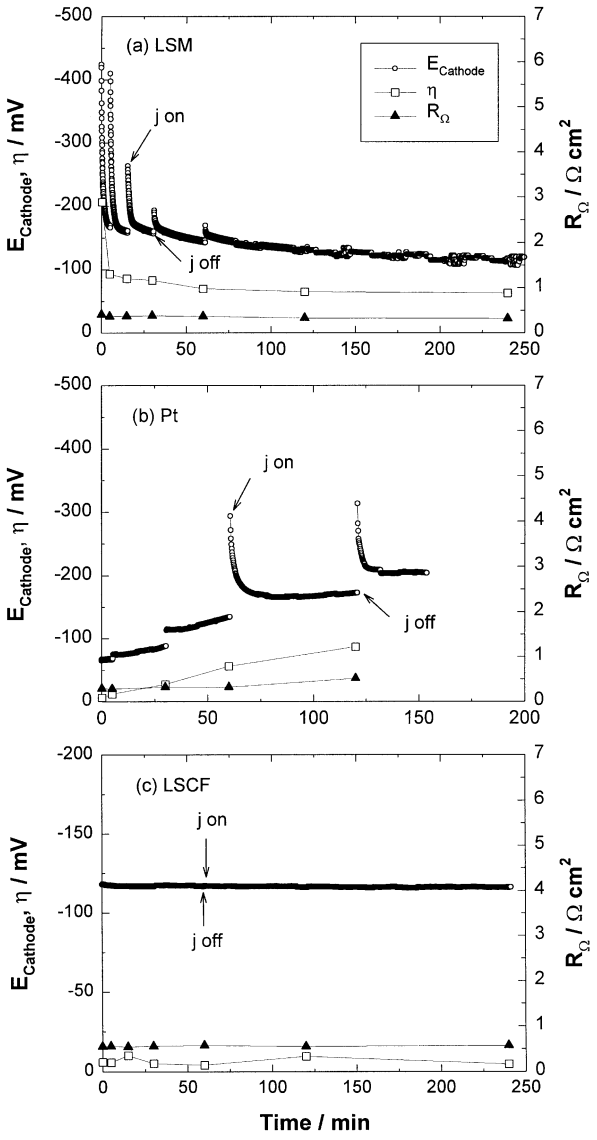

Fig. 3. Initial polarization curves of (a) LSM, (b) Pt and (c) LSCF electrodes for O_2 reduction in the absence of chromia-forming alloy interconnect at 200 mA cm^{-2} and 900 °C.

current passage treatment). However, $E_{Cathode}$ increased steadily with the current passage time and after the current passage for 60 min, $E_{Cathode}$ developed a distinct polarization potential behavior similar to that observed for the LSM electrode (Fig. 3b). The $E_{Cathode}$ started at a high value and decreased rapidly with the cathodic current passage. The high $E_{Cathode}$ value after polarized for 60 min could be due to the inhibiting effect of Pt–O species formed on the Pt electrode surface on the O_2 reduction reaction, and the rapid reduction in $E_{Cathode}$ with the cathodic current passage is an indication of the reduction of Pt–O species on the electrode surface, as shown by Sridhar et al.[20] The simultaneous increase in R_Ω with the cathodic current passage time probably indicates that the deterioration of the electrochemical activities of the Pt electrodes is also related to the low

sinterability of thin Pt coatings at high temperatures.[21] Very different to that on LSM and Pt electrodes, the polarization potential for the reaction on the LSCF electrode was very stable and did not change with the current passage (Fig. 3c). LSCF electrode had very low η (<10 mV at 200 mA cm^{-2}), indicating high electrochemical activity for O_2 reduction reactions. The high electrochemical activity for the O_2 reduction is most likely related to the high mixed ionic and electronic conductivities of LSCF materials in comparison with the dominant electronic conductivities of LSM and Pt materials.[22–24]

Fig. 4 shows the initial polarization behavior of LSM, Pt and LSCF electrodes for O_2 reduction at 200 mA cm^{-2} and 900 °C in the presence of chromia-forming alloy interconnect. The time behavior of $E_{Cathode}$ for the reaction on the electrodes studied was remarkably different from that in the absence of chromia-forming alloy. Instead of rapid decrease in the absence of chromia-forming alloy, $E_{Cathode}$ increased rapidly initially with cathodic current passage, followed by a region where the increase in $E_{Cathode}$ was much slower for the reaction in the presence of chromia-forming alloy interconnect. The initial increase in $E_{Cathode}$ was very high on LSM and Pt electrodes while for the reaction on the LSCF electrode it was much smaller. The change of $E_{Cathode}$ with the current passage time is almost fully reproducible, an indication of strong inhibiting effect of the gaseous Cr species on the surface process such as the dissociative adsorption and diffusion reaction on the electrode surface for the O_2 reduction at early stages of the polarization.[14,25]

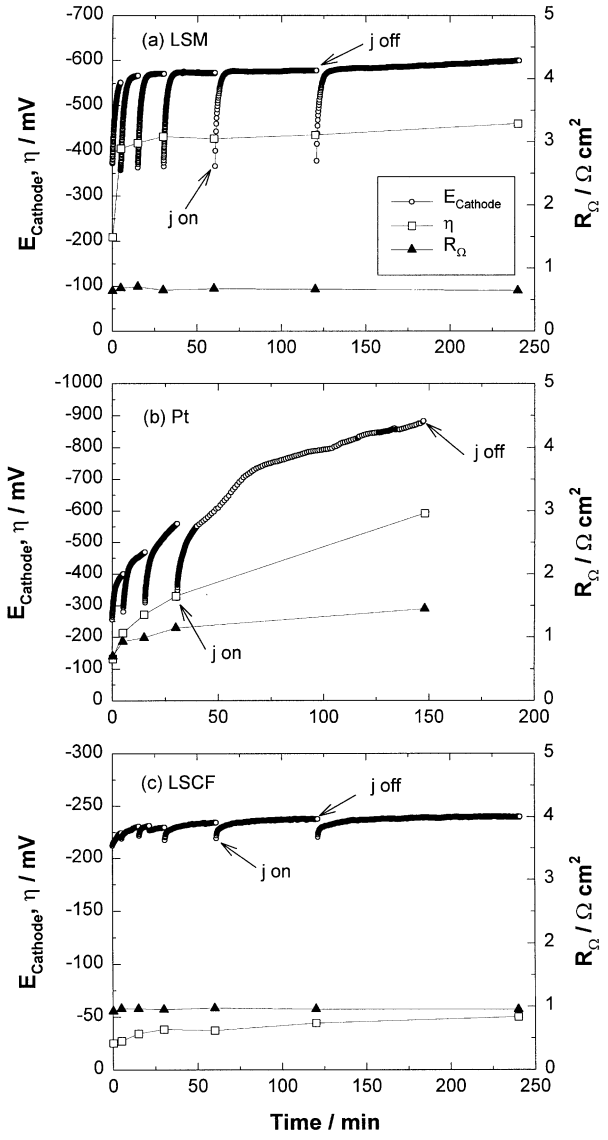

Fig. 4. Initial polarization curves of (a) LSM, (b) Pt and (c) LSCF electrodes for O_2 reduction in the presence of chromia-forming alloy interconnect at 200 mA cm^{-2} and 900 °C.

3.2. Deposition of Cr species

Fig. 5 is the SEM micrograph of exposed TZ3Y electrolyte surface after the LSM electrode coating was carefully removed and EDS pattern of crystals formed on the TZ3Y electrolyte surface. LSM electrode was polarized at 200 mA cm^{-2} and 900 °C for 4 h in the presence of chromia-forming alloy. Particles with irregular shape were LSM particles left on the TZ3Y electrolyte

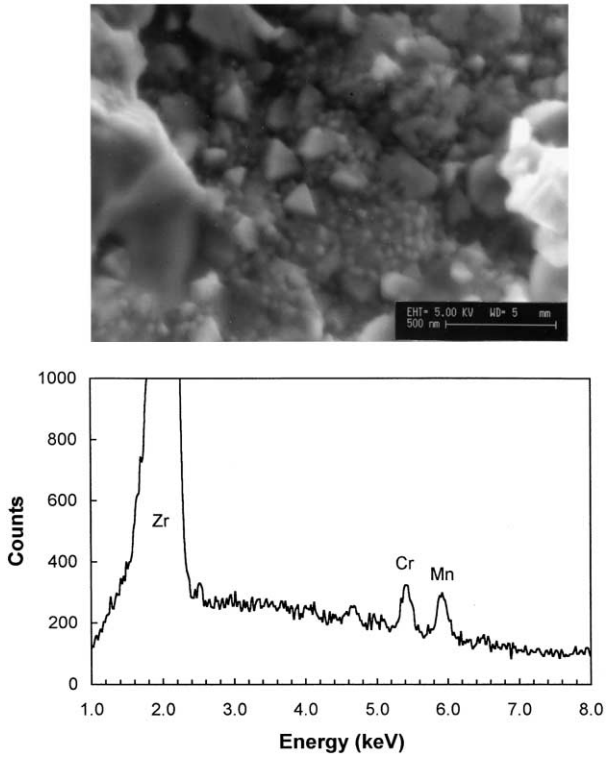

Fig. 5. SEM micrograph of exposed TZ3Y electrolyte surface after LSM electrode coating was removed and EDS pattern of crystals deposited on the TZ3Y electrolyte surface. The LSM electrode was polarized at 200 mA cm^{-2} and 900 °C in the presence of the chromia-forming alloy for 4 h.

surface. On the electrolyte surface between LSM particles, there were fine grains (ca. 0.05 μm) and relatively large crystals (ca. 0.17 μm). The crystals formed have developed distinct facets, similar to that of $(Cr,Mn)_3O_4$ spinels.[11] EDS analysis showed that the crystals contain Cr and Mn, indicating that they are most likely $(Cr,Mn)_3O_4$ spinel phase. Deposition of Cr species (fine grains and large crystals) occurred not only on the areas adjacent to the LSM/electrolyte interface regions but also on the whole TZ3Y electrolyte surface areas between LSM particles. However, for LSM particles in contact with the TZ3Y electrolyte surface, EDS did not detect Cr species within the limit of the technique. Deposition of Cr species was not detected on the LSM electrode surface or inside the electrode bulk. The results indicate that deposition of Cr species preferentially occurs on the electrolyte surface at early stages of polarization.

Fig. 6 shows the SEM micrographs of a LSM electrode after cathodic polarization at 200 mA cm^{-2} and 900°C for 129 h. On the TZ3Y electrolyte surface, there was a formation of a deposit ring at the edge of the LSM electrode (Fig. 6a). The average ring width was ca. 89 μm. For the electrode polarized for 50 h, the ring was ca. 60 μm wide.[13] The morphology and distribution of Cr deposits over the deposit ring area were identical for

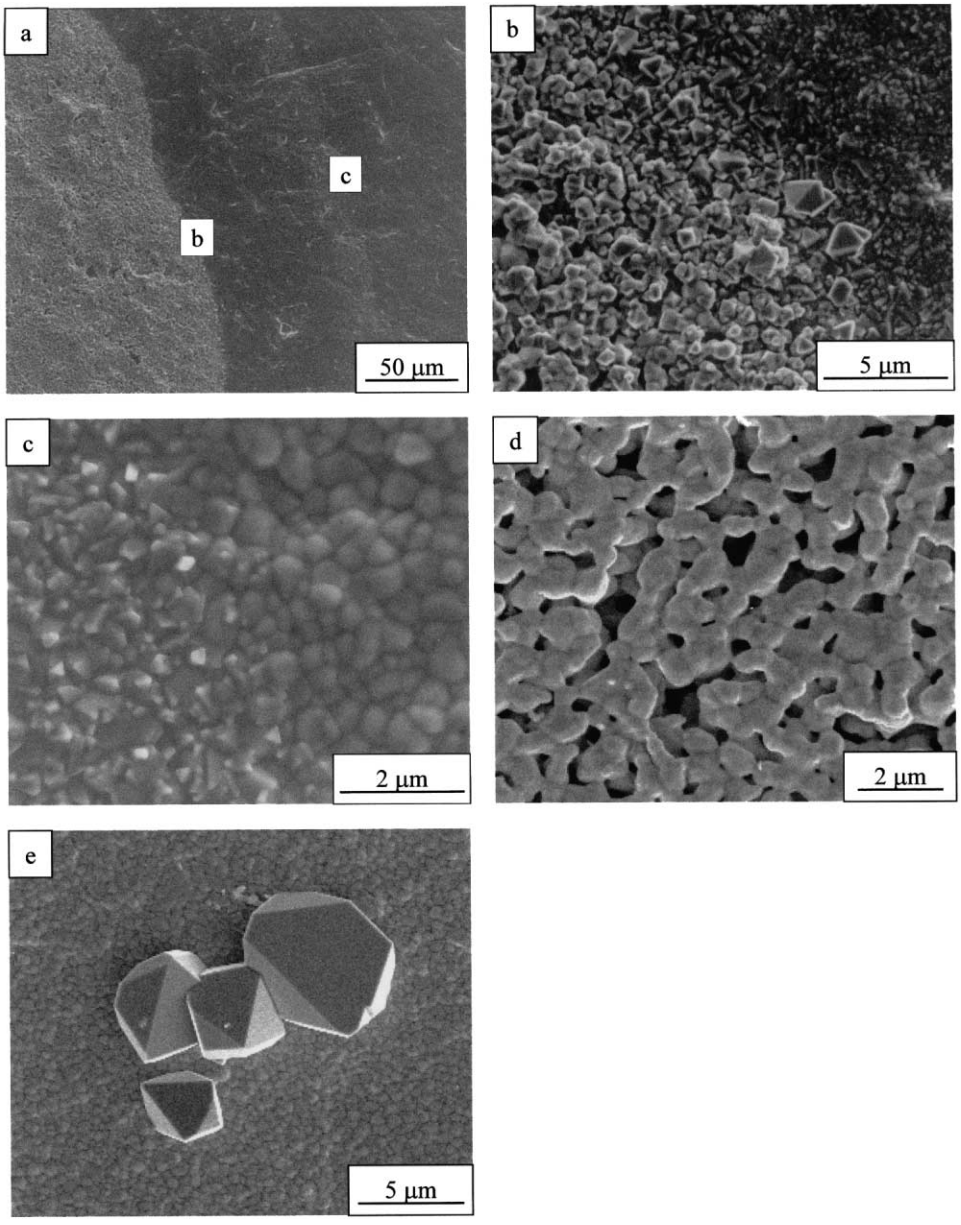

Fig. 6. SEM micrographs of a LSM electrode after polarized at 200 mA cm^{-2} and 900 °C in the presence of chromia-forming alloy for 129 h. (a) the overall view of the electrode, showing the formation of a deposit ring at the edge of the electrode, (b) ring area next to the LSM electrode, (c) ring areas close to the clean TZ3Y electrolyte surface, (d) LSM electrode surface and (e) isolated deposits on the LSM electrode surface.

the LSM electrode polarized at 200 mA cm^{-2} and 900 °C for 50 h.[13] In the ring areas close to the edge of the LSM electrode, the deposits were mainly fine grains and crystals (Fig. 6b). In the ring areas close to the clean TZ3Y electrolyte surface side, the deposit layer consisted of only crystals (Fig. 6c). There was a clear boundary between the deposit ring and TZ3Y electrolyte. The surface of the LSM electrode was in general very clean with no visible deposition of either fine grains or crystals (Fig. 6d). However, in some isolated spots, large individual particles were found on the LSM electrode surface (Fig. 6e). Fig. 7a shows EDS pattern of Cr deposits at areas close to the edge of the LSM electrode (fine grains and crystals) and Fig. 7b the EDS pattern of Cr deposits at areas close to edge of the clean TZ3Y electrolyte surface (crystals). Over the whole deposit ring area, deposits contain only Cr and Mn. Cr content in respect to that of Mn was higher at the area close to the edge of the LSM electrode than the area close to the edge of the clean TZ3Y electrolyte surface. The relatively high Cr content is consistent with the observation of the formation of fine Cr_2O_3 grains and $(Cr,Mn)_3O_4$-type spinel crystals at areas close to the edge of LSM electrode.[13] The EDS analysis of the clean LSM electrode surface as shown in Fig. 6d was typical patterns for LSM materials, indicating there is no Cr deposition on the LSM electrode surface after polarization at 900 °C for 129 h (Fig. 7c). Fig. 7d is the EDS analysis of the particles formed on the electrode surface, showing the presence of Cr only. This indicates that the composition of isolated Cr particles formed on the surface is most likely Cr_2O_3.

Fig. 8 is the SEM micrographs of a Pt electrode in contact with chromia-forming alloy interconnect after polarization at 200 mA cm^{-2} and 900 °C for 22 h and typical EDS analysis of small and large particles on the TZ3Y electrolyte surface. The sphere-like large particles were Pt particles. EDS analysis of small particles on the TZ3Y electrolyte surface show the presence of Pt only (Fig. 8c). Very different from that observed on the LSM electrode (see Figs. 5 and 6), there was no formation of fine grains or particles with clear crystal facets on the TZ3Y electrolyte surface despite the fact that Pt electrode was polarized for 22 h, considerably longer than the 4 h period used for the LSM electrode shown in Fig. 5. There was also no deposition of fine grains or particles on the Pt electrode surface. Occasionally, there were one or two isolated Cr deposit particles on the TZ3Y electrolyte surface and EDS showed the presence of Cr and Fe. This indicates that such Cr deposits are most likely due to the direct contact between the chromia alloy and the TZ3Y electrolyte surface. However, in general the TZ3Y electrolyte surface and Pt electrode surface were clean and almost free of Cr deposits for the O_2 reduction at Pt electrode under the conditions studied. This indicates that the deposition of Cr species at Pt electrodes in the presence of chromia-forming alloy is kinetically inhibited, compared to that at LSM electrodes under identical polarization conditions.

Fig. 9 is the SEM micrographs of a LSCF electrode in the presence of chromia-forming alloy interconnect after polarization at 200 mA cm^{-2} and 900 °C for 105 h. On the LSCF electrode surface, there was deposition of particles with distinct crystal facets and the size of the

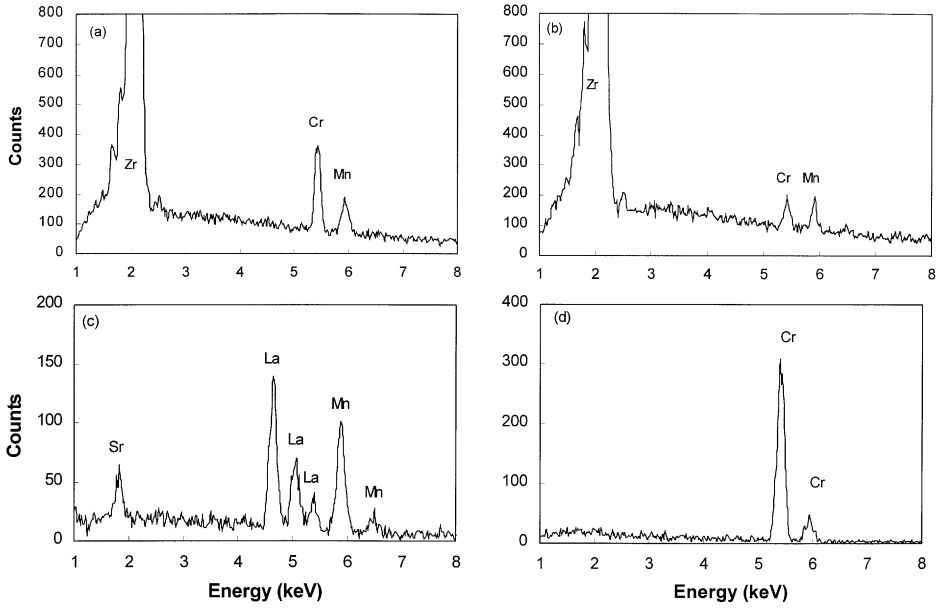

Fig. 7. EDS patterns of the LSM electrode shown in Fig. 6. (a) Deposits on the ring areas next to the edge of the LSM electrode (Fig. 6b). (b) Deposits on the ring areas close to the clean TZ3Y electrolyte surface (Fig. 6c). (c) LSM electrode surface (Fig. 6d) and (d) isolate deposit particles on the LSM electrode surface (Fig. 6e).

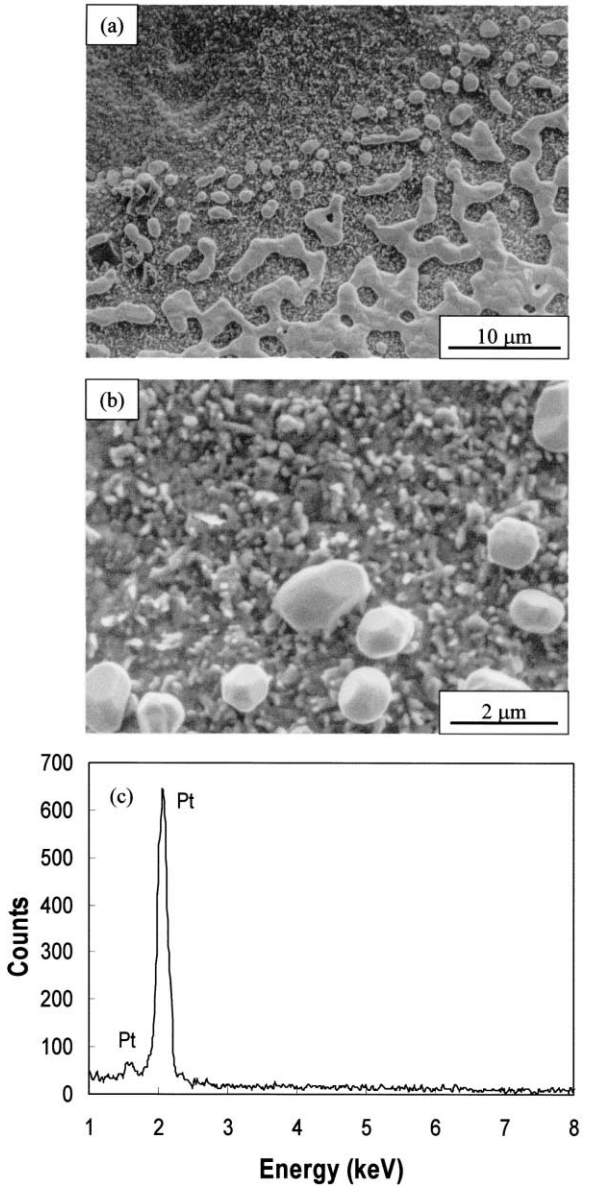

Fig. 8. SEM micrographs of a Pt electrode after polarized at 200 mAcm^{-2} and 900 °C in the presence of chromia-forming alloy for 22 h and typical EDS patterns of large and small particles on the TZ3Y electrolyte surface.

particle was in the range of 0.7–3.5 μm, significantly higher than the grain size of LSCF particles (ca. 0.11 μm). The particles grew from the LSCF coating. There was no visible difference in the deposition of Cr species on the electrode surface under the channel and the rib of the chromia-forming alloy. On SDC electrolyte surface there was also formation of Cr deposit particles (Fig. 9b). Very different from that observed for the deposition of Cr species at LSM electrodes, the deposition of Cr species appears to be random in nature and did not show any preferential deposition either on the electrolyte surface or on the electrode surface. Fig. 10 is the EDS patterns of the particles deposited on the

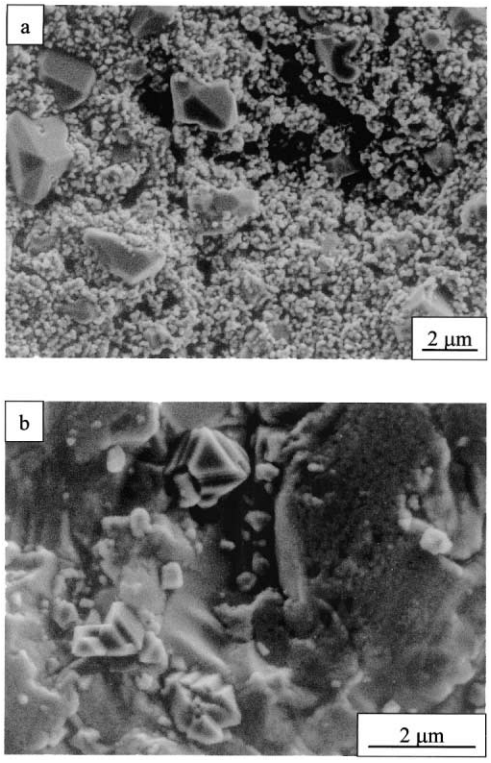

Fig. 9. SEM micrographs of a LSCF electrode after polarized at 200 mA cm^{-2} and 900 °C in the presence of chromia-forming alloy for 105 h. (a) LSCF electrode surface and (b) SDC electrolyte surface.

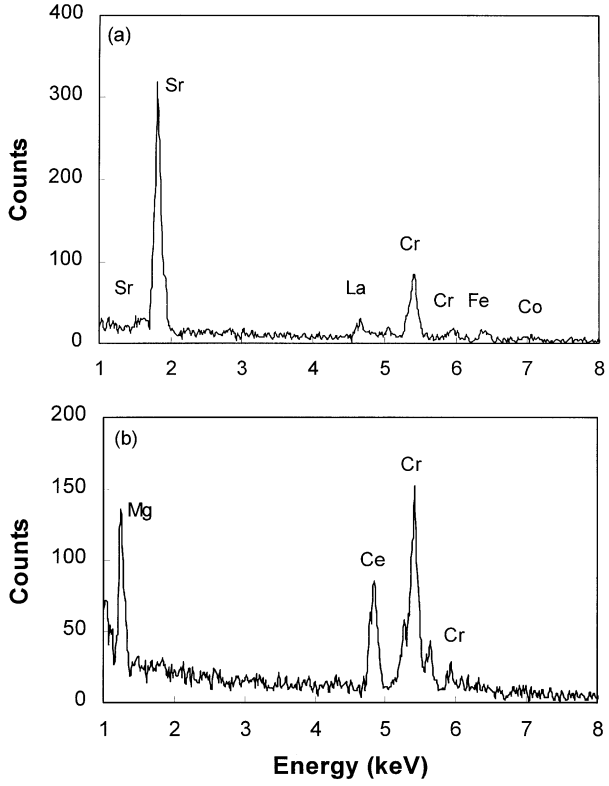

Fig. 10. EDS patterns of the LSCF electrode shown in Fig. 9. (a) Deposit particles on the LSCF electrode (Fig. 9a) and (b) deposit particles on the SDC electrolyte surface (Fig. 9b).

LSCF electrode surface and on the SDC electrolyte surface. Particles formed on the LSCF electrode surface primarily contained Sr and Cr with minor La, Co and Fe (Fig. 10a). The high intensity of Sr indicates high Sr content in the particles deposited on the LSCF electrode surface. For the particles on the SDC electrolyte, EDS analysis indicates the presence of Cr, Ce and Mg (Fig. 10b). The fact that Mg was only found on the deposit particles on the SDC electrolyte surface and not on the deposit particles on the LSCF electrode surface shows that Mg may come from the contamination during the SDC electrolyte substrate preparation. The formation of individual particles rather than covering the whole electrolyte surface may indicate that CeO_2 is not an effect nucleation agent for Cr deposition as that of Mg species. Considering that the polarization conditions for LSM and LSCF electrodes were very similar, the characteristics of the Cr deposition for the O_2 reduction on the LSCF electrode are remarkably different from that on the LSM electrode.

For the LSCF electrode in contact with the chromia-forming alloy after heating at 900°C for 140 h in the absence of polarization potentials, there were clear contact marks formed on the electrode coating surface. By naked eye, the LSCF electrode surface area under the rib of the Cr alloy interconnect was black in color and the area under the channel of the Cr alloy interconnect was green in color. The green color indicates the high deposition of Cr species on the electrode surface area under the channel of the Cr alloy. Fig. 11 shows the details of the LSCF electrode surface area under the channel and the rib of the alloy and the SDC electrolyte surface. On the LSCF electrode surface under the channel of the chromia-forming alloy, there was significant Cr deposition and grain growth (Fig. 11a). The electrode surface was completely covered by the Cr deposits. On the electrode surface under the rib of the chromia-forming alloy, the deposit particles were not continuous and fine LSCF particles can still be seen on the electrode surface (Fig. 11b). Deposition of Cr species on the LSCF electrode surface under the rib of the chromia-forming alloy was much lower than that under the channel of the alloy, consistent with the appearance of the electrode coating after the heat treatment. On the SDC electrolyte surface, there was formation of deposit particles, similar to that of the LSCF electrode after polarized at 900 °C and 200 mA cm^{-2} for 105 h. Fig. 12 shows the EDS patterns of the particles formed on the LSCF electrode surface area under the channel and rib of the chromia-forming alloy. On the LSCF electrode surface under the channel of the alloy, the deposits contain only Sr and Cr with significantly higher Sr content compared to that of Cr (Fig. 12a). For the particles on the LSCF electrode surface under the rib of the alloy, the deposit contains Cr, Sr, La, Co and Fe. The sulphur detected in the deposit particles may come from the environment of the

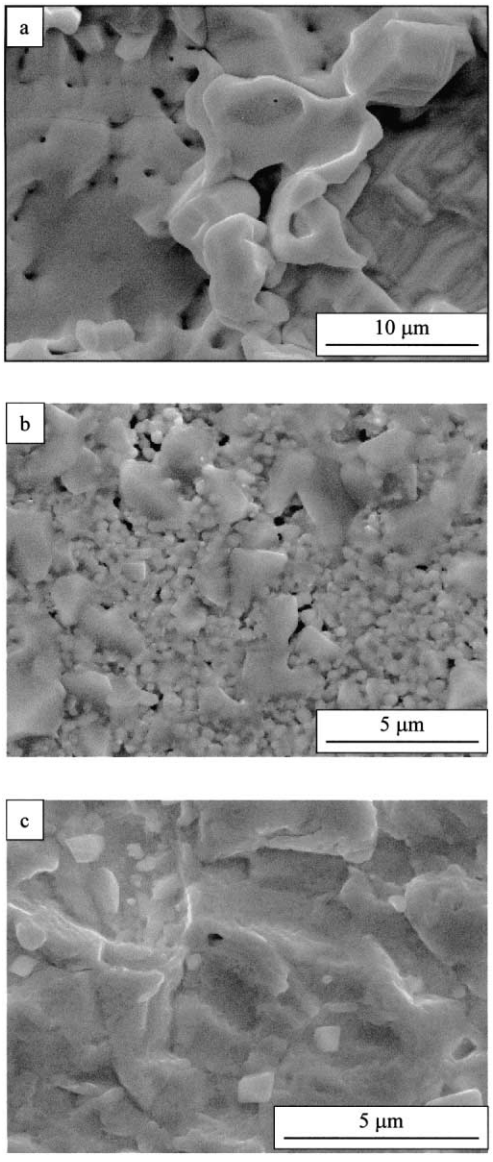

Fig. 11. SEM micrographs of a LSCF electrode heated at 900 °C in the presence of the chromia-forming alloy for 140 h with no polarization. (a) LSCF electrode surface under the channel of the Cr alloy, (b) LSCF electrode surface under rib of the Cr alloy and (c) SDC electrolyte surface.

furnace during the heating treatment. The transportation of Cr species to the LSCF electrode surface is probably dominated by solid phase diffusion of Cr species under the rib of the alloy while that under the channel of the alloy is dominated by the vapor phase diffusion of gaseous Cr species. The significant difference in the quantities in the Cr deposition on the LSCF electrode under the rib and channel of the alloy indicates that vapor phase diffusion of Cr species would be much faster and more significant than the solid phase diffusion under the conditions studied. The distribution and the characteristics of the deposit particles on the SDC electrolyte surface were similar to that for the LSCF electrode after polarized at 200 mA cm^{-2} for 105 h. The

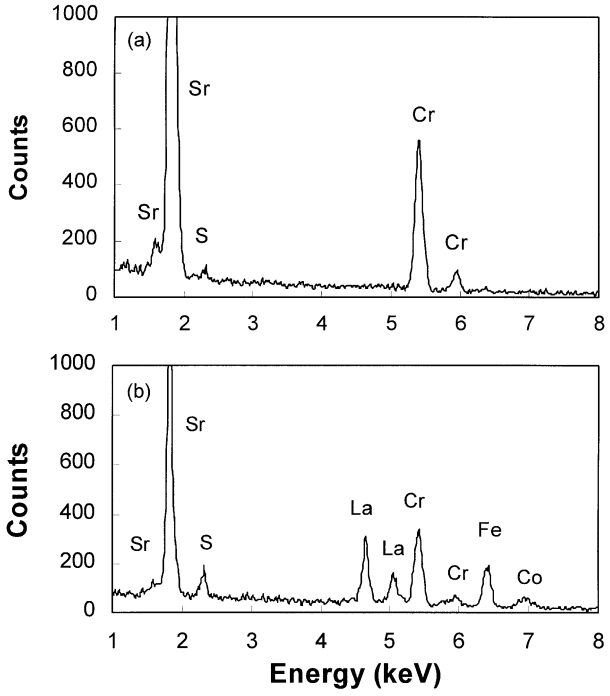

Fig. 12. EDS patterns of the LSCF electrode shown in Fig. 11. (a) Deposits on the LSCF electrode surface under the channel of the Cr alloy and (b) deposits on the LSCF electrode surface under the rib of the Cr alloy.

EDS patterns of the Cr deposits on the SDC electrolyte surface were exactly the same as that observed on the SDC electrolyte surface of the LSCF electrode after polarization for 105 h. This indicates that the deposition of Cr species on the SDC electrolyte surface is not affected by the presence and absence of cathodic polarization.

3.3. Effect of electrode materials on the Cr deposition process

As shown earlier,[13–15] the deposition process of Cr species at LSM electrodes is not controlled by the electrochemical reduction reaction of high valent Cr species in competition with O_2 reduction. The deposition of Cr species is essentially dominated by the chemical dissociation reaction on re-deposition. The evidences to support the chemical nature of the deposition process of Cr species at LSM electrodes are summarized as follows. (1) The deposition of Cr species on the TZ3Y electrolyte surface took place under both cathodic and anodic polarization potentials [13]. This indicates that deposition of Cr species at LSM electrode is not dominated by the electrochemical reduction of high valent Cr species. Under cathodic polarization, a deposit ring was formed on the TZ3Y electrolyte surface around the edge of the LSM electrode. The ring was ca. 60 μm for the electrode polarized at 200 mA cm^{-2} and 900 °C for 50 h and ca. 89 μm for 129 h (Fig. 6). The deposit ring is substantially wider than the width of the three phase boundary (TPB) region for the O_2 reduction on LSM electrode, which is estimated to be less than 1 μm.[26] On the other hand, the electrode interface resistance (R_E) measured by the electrochemical impedance spectroscopy at open circuit did not change much with the current passage at early stages of polarization, indicating that the O_2 reduction reaction still proceeds through the electrode/electrolyte interface region despite the significant deposition of Cr species on the zirconia electrolyte surface.[12,14] This shows that the deposition of Cr species is not limited to a narrow TPB region. (2) The characteristics of the Cr deposition at the LSM electrode are significantly affected by the air flow for the O_2 reduction in the presence of chromia-forming alloy.[15] Under air flow, Cr preferentially deposited on the TZ3Y electrolyte surface while on the LSM electrode surface or inside the LSM electrode bulk, there was no Cr deposition for the LSM electrode polarized at 200 mA cm^{-2} and 900 °C for 50 h.[13] For a LSM electrode polarized at 200 mA cm^{-2} and 900 °C for 4 h with no air flow, the Cr deposition took place on the TZ3Y electrolyte surface and on the LSM electrode surface.[15] On the TZ3Y electrolyte surface under the rib of the Cr alloy, a deposit band of fine grains and particles was formed and was as wide as ca. 300 μm while on the TZ3Y electrolyte surface under the channel of the interconnect, the density of the deposits was very low and there was no formation of deposit band. The substantial difference in the characteristics of the Cr deposition associated with the geometrical space between the interconnect and the electrolyte surface in the case of no air flow cannot be explained by the electrochemical mechanism of the deposition of Cr species. (3) In the absence of polarization potentials, deposition of Cr species occurred on the TZ3Y electrolyte surface when heated at 1100 °C for 50 h but not at 900C.[13] This indicates that the temperature as well as polarization potentials can significantly promote the deposition process of Cr species at LSM electrodes. (4) Finally, for the O_2 reduction at LSM electrodes in the presence of the chromia-forming alloy, the surface process of the reaction is inhibited by the gaseous Cr species while the oxygen migration/diffusion into the electrolyte is inhibited by the Cr species deposited on the electrolyte surface.[14] The Cr deposit ring on the electrolyte surface grew with the deposition time and the reaction became increasingly dominated by the inhibiting effect of the Cr deposits on the oxygen migration and diffusion process into the electrolyte. This in turn explains the observed correlation between the performance degradation and the accumulation of the Cr species at the electrode/electrolyte interface region.[10]

For the O_2 reaction in the presence of the chromia-forming alloy, there were similarities between the polarization behavior of Pt and LSM electrodes. $E_{Cathode}$ was characterized by a rapid initial increase, followed by a

relatively slow increase with current passage time. The relatively fast increase of $E_{Cathode}$ for the O_2 reduction on Pt electrodes is probably related to the rapid deterioration of the Pt electrode microstructure at high temperatures. Similar electrode behavior could be related to the fact that oxygen ion conductivity of both Pt and LSM materials is very low. At 900 °C the oxygen diffusion coefficient of LSM materials is in the range of 10^{-12}–10^{-14} cm^2 s^{-1}.[22,23] For Pt materials, the oxygen diffusion coefficient extrapolated from high temperature values could be as low as 10^{-19} cm^2 s^{-1} at 900 °C.[24] On cone-shaped LSM electrodes, Siebert et al.[27] show that the LSM electrode behaves like a metal electrode at low polarization potentials. This appears to be indicated by the development of a two distinct polarization potential regions for the reaction on the Pt electrode after current passage for 60 min, similar to that of the LSM electrode for the O_2 reduction in the absence of chromia-forming alloy (Fig. 3). Similar to that on LSM electrodes,[25,27–29] O_2 reduction on Pt electrodes is predominantly controlled by the surface process kinetics and the reaction occurs mainly at the TPB region.[25,30,31] However, the characteristics of the deposition of Cr species are very different at LSM and Pt electrodes in the presence of the chromia-forming alloy. As shown in Fig. 4, for the O_2 reduction at the LSM electrode after being polarized for 4 h, there was a considerable deposition of Cr species of fine grains and large crystals on the TZ3Y electrolyte surface. In contrast to the Cr deposition at LSM electrodes, there was no detectable deposition of Cr species (fine grains or deposit crystals) either on the TZ3Y electrolyte or on the Pt electrode surface (Fig. 8) despite the fact that Pt electrode was polarized at 200 mA cm^{-2} and 900 °C for 22 h, much longer than the 4 h for the LSM electrode. The remarkable different characteristics of the deposition of Cr species at the Pt and LSM electrodes is in sharp contrast to the similar electrode behavior for the reaction in the presence of chromia-forming alloy. This indicates that the deposition of Cr species at Pt electrodes is not controlled by the electrochemical reduction of high valent Cr species to Cr_2O_3 in competition with O_2 reduction reactions under SOFC operation conditions. The very different characteristics of the deposition of Cr species at Pt and LSM electrodes under similar experimental conditions also show that the kinetics of the deposition strongly depends on the electrode material.

The non-electrochemical nature of the deposition processes of Cr species under SOFC operation conditions is also supported by the deposition behavior of Cr species on the LSCF electrode. The electronic conductivity of LSCF materials is ca. 180 S cm^{-1} at 900 °C,[32] close to ca. 200 S cm^{-1} at 900 °C of the LSM material.[33] However, the oxygen ion conductivity of LSCF is much higher than that of the LSM. At 900 °C, for LSCF with composition of $La_{0.5}Sr_{0.5}Co_{0.8}Fe_{0.2}O_3$, the oxygen diffusion coefficient is ca. 5×10^{-7} cm^2 s^{-1},[22] much higher than 10^{-12}–10^{-14} cm^2 s^{-1} of LSM materials.[22,23] The high oxygen ion conductivity of LSCF materials could be the main reason for the much higher electrochemical activity for the O_2 reduction in the absence and presence of chromia-forming alloy in comparison to that of the LSM electrode, e.g., low η, stable $E_{Cathode}$ and much smaller increase in the $E_{Cathode}$ for the reaction in the presence of the chromia-forming alloy. As shown elsewhere,[25] the much smaller increase in $E_{Cathode}$ and very low η for the reaction on the LSCF electrode as compared to that on LSM and Pt electrodes indicates that the surface process plays much smaller role in the overall reaction kinetics than that of the bulk diffusion process. Thus, in terms of the contribution of the surface and bulk diffusion processes to the overall O_2 reduction kinetics the difference in the electrode process between LSCF and LSM electrodes would be primarily quantitative, i.e. the surface process kinetics play a dominant role for the reaction on the LSM electrode and to a much less extent on the LSCF electrode.

However, the characteristics of the deposition of Cr species at LSCF electrodes are not only quantitatively but also qualitatively different from that at LSM electrodes. For a LSCF electrode polarized at 200 mA cm^{-2} in the presence of the chromia-forming alloy for 105 h at 900°C, there was no preferential deposition of Cr species on the SDC electrolyte surface close to the edge of the LSCF electrode. As shown above, the deposition of Cr particles on the SDC electrolyte surface is most likely caused by the Mg impurities on the SDC electrolyte surface and is independent of the polarization. Deposition of Cr species occurred on the LSCF electrode surface, forming deposit particles containing Sr–Cr–La–Co–Fe (Fig. 9a). This is very different from the observation that for the LSM electrode under the same polarization conditions for 129 h, the electrode surface was basically very clean except a few isolated Cr deposits (Fig. 6d). For LSM electrode heated at 900 °C for 50 h in the absence of polarization, there was no deposition of Cr species either on the TZ3Y electrolyte surface or on the LSM electrode surface.[13] For the LSCF electrode heated at 900°C in the absence of polarization for 140 h, there was significant deposition of Cr species on the LSCF electrode surface, completely covering the surface under the channel of the chromia-forming alloy. Even taking into account the difference in the time for the LSCF electrode treated in the presence and absence of polarization at 900 °C, it appears that the deposition of Cr species was more pronounced at LSCF electrode in the absence of polarization than that in the presence of polarization at 900 °C (see Figs. 9a and 11a). This demonstrates that the deposition of Cr species at LSCF electrodes cannot be an electrochemical reduction of high valent Cr species in competition with O_2 reduction reactions, consistent with the proposed deposition

mechanism of the Cr deposition process at LSM and Pt electrodes. The very different characteristics of the Cr deposition at LSCF electrodes compared to that at LSM electrode indicate that the nucleation agent (i.e. the nucleation sites) for the nuclei formation and Cr deposition at the LSCF electrode is very different from that at LSM electrodes.

3.4. Driving force for the deposition of Cr species

Under cathodic polarization potentials, Mn in the LSM lattice and interstitial sites can be electrochemically reduced to Mn^{2+} species, forming concomitantly oxygen vacancies.[34] As shown early,[13,15] the driving force for the deposition of Cr species at LSM electrodes is most likely Mn^{2+} species generated under cathodic polarization[34] or at high temperatures.[35] Mn^{2+} species generated react with gaseous Cr species, forming Cr–Mn–O nuclei and subsequently leading to the Cr_2O_3 grain growth and $(Cr,Mn)_3O_4$ spinel formation. The kinetics of the deposition processes of Cr species is, therefore, controlled by the nucleation reaction between the Mn^{2+} and the gaseous Cr species.[13,15] The flux of gaseous Cr species is most affected by the temperature, pressure and the geometric factor such as steps or corners on the TZ3Y electrolyte surface at the edge of the LSM electrode and the space between the substrate surface and the interconnect. The effect of the geometric factor on the deposition of Cr species is clearly demonstrated by the substantial deposition of Cr species on the TZ3Y electrolyte surface under the rib of the interconnect compared to that under the channel of the interconnect in the case of no air flow.[15]

For the O_2 reduction at LSCF electrodes in the presence of chromia-forming alloy, deposition of Cr species occurred primarily on the LSCF electrode (deposition of Cr particles on SDC electrolyte surface is most likely due to presence of the Mg impurities and thus will not be discussed here). EDS analysis indicated that deposits on the LSCF electrode surface in the presence and absence of polarization primarily contain Cr and Sr, indicating that the nucleation agent for the Cr–Sr–O nuclei formation is most likely associated with the SrO species on the LSCF electrode surface. The SrO as nucleation agent in the case of LSCF electrode is also consistent with the chemical stability results of the $(La,Sr)CoO_3$ (LSC) layer plasma sprayed on the chromia-forming alloy, reported by Quadakkers et al.[5] For the specimen coated with LSC layer after heat treatment at 950°C for 1000 h, Sr was segregated to the interface between the alloy and the LSC layer and almost no Sr was left inside the LSC layer. The EPMA analysis showed the interface product of $SrCrO_4$ between the alloy and LSC layer. $SrCrO_4$ oxides had a columnar structure growing from the LSC coating in the direction of the alloy surface. The formation of $SrCrO_4$ and $LaCrO_4$ was also observed on the surface of LSCF pellets in contact with gaseous Cr species at temperatures as low as 750°C in the absence of polarization.[36] Miura et al.[37] reported that acid etching of LSCF membrane significantly improved the oxygen permeability of the membrane and XPS analysis showed that acid etching mainly reduced the SrO content on the membrane surface. This indicates that SrO may be enriched at the surface of LSCF materials. Recent study showed that cathodic current/polarization treatment can significantly enhance the LSM electrode performance probably through the decrease and/or removal of SrO species initially enriched at the active sites on the LSM electrode surface.[38] In contrast to the Mn^{2+} species generation under cathodic polarization,[34] cathodic polarization may actually have a cleaning effect on the SrO content originally segregated on the LSM and LSCF electrode surface.[38] This could lead to the reduction in the nucleation reaction between the SrO and the gaseous Cr species on the LSCF electrode surface. The cleaning effect of the cathodic polarization on SrO content on the LSCF surface could be the reason for the observed much less deposition of Cr species on the LSCF electrode in the presence of current passage of 200 mA cm^{-2} than that on the LSCF electrode surface under the channel in the absence of current passage. The effect of the cathodic polarization on the deposition of Cr species on the LSCF electrode appears to be opposite to that on the LSM electrode, another evidence that the deposition of Cr species at SOFC cathodes is not an electrochemical reduction of high valent Cr species in competition with O_2 reduction.

Very different to that at LSM and LSCF electrodes, deposition of Cr species for the O_2 reduction at Pt electrodes was extremely small. There was no detectable deposition of Cr fine grains or crystals either on the TZ3Y electrolyte surface or on the Pt electrode surface for the Pt electrode polarized at 200 mA cm^{-2} and 900 °C for 22 h (Fig. 8). This indicates that Pt itself is a very poor nucleation agent for the deposition of gaseous Cr species and thus there are no sufficient nucleation sites for the chemical dissociation of high valent Cr oxide species such as CrO_3 to form Cr_2O_3. The in turn shows that the direct dissociation reaction of CrO_3 to form Cr_2O_3 is not kinetically favorable at the TZ3Y electrolyte surface at 900 °C, consistent with the results on the LSM electrode/TZ3Y electrolyte system in the absence of polarization.[13] The inert nature of Pt on the nucleation and deposition of Cr species could also explain the much lower oxidation rate of a chromia-forming alloy coated with Pt compared to that coated with LSC, as reported by Hou et al.[39]

4. Conclusions

Deposition processes of Cr species have been investigated for the O_2 reduction at LSM, Pt and LSCF

electrodes at 900°C. In the chromia-forming alloy interconnect/LSM electrode/TZ3Y electrolyte cell, Cr deposition took place preferentially on the TZ3Y electrolyte surface with the formation of Cr_2O_3 fine grains and $(Cr,Mn)_3O_4$ spinel crystals while in the chromia-forming alloy interconnect/LSCF electrode/SDC electrolyte cell, deposition of Cr species primarily occurred on the LSCF electrode surface, forming Cr oxides with very high Sr content. In contrast, in the chromia-forming alloy interconnect/Pt electrode/TZ3Y electrolyte cell, there was no significant deposition of Cr species either on the TZ3Y electrolyte surface or on the Pt electrode surface. The results conclusively demonstrated that the deposition of Cr species at SOFC cathodes is not controlled by the electrochemical reaction at the TPB region and thus is not an electrochemical reduction of high valent chromium vapor species such as CrO_3 to solid Cr_2O_3 in competition with O_2 reduction. Deposition of Cr species is essentially a chemical dissociation process on re-deposition. The driving force for the deposition of Cr species is associated with the nucleation reaction between nucleation agent and gaseous Cr species. At LSM electrodes, the nucleation agent is the Mn species in particular Mn^{2+} ions generated under cathodic polarization potentials or at high temperatures. At LSCF electrodes, the nucleation agent is the SrO species either originally enriched at the LSCF electrode surface and/or from the LSCF perovskite structure. On the other hand Pt is a poor nucleation agent for the deposition of Cr species. The presence of impurities such as Mg in the system could also significantly enhance the deposition process of Cr species.

Acknowledgements

The technical help from Jason Baigent, Todd Byrnes and Kylie Chapman for the preparation of TZ3Y electrolytes, chromia-forming alloy interconnect coupons and LSM electrodes is greatly appreciated. Work was performed at Ceramic Fuel Cells Ltd., Australia.

References

1. Donelson, R., Amarasinghe, S., Goble, D., Hickey, D., Jiang, S. P., Love, J. and Quach, T., Intermediate temperature solid oxide fuel cell technology. In *Proceedings of the 3rd European Solid Oxide Fuel Cell Forum*, ed. P. Stevens. European Fuel Cell Group, Nantes, France, 1998.
2. Murray, E. P., Tsai, T. and Barnett, S. A., A direct-methane fuel cell with a ceria-based anode. *Nature,* 1999, **400**, 649–651.
3. Minh, N. Q. and Montgomery, K., Performance of reduced-temperature SOFC stacks. In *SOFC-V, PV 97-40*, ed. U. Stimming, S. C. Singhal, H. Tagawa and W. Lehnert. The Electrochemical Society, Pennington, NJ, 1997, pp. 153–159.
4. Ivers-Tiffee, H., Wersing, W., Schieβl, M. and Greiner, H., Ceramic and metallic components for a planar SOFC. *Ber. Bunsenges. Phys. Chem.,* 1990, **94**, 978–981.
5. Quadakkers, W. J., Greiner, H., Hänsel, M., Pattanaik, A., Khanna, A. S. and Malléner, M., Compatibility of perovskite contact layers between cathode and metallic interconnector plates of SOFCs. *Solid State Ionics,* 1996, **91**, 55–67.
6. Das, D., Miller, M., Nickel, H. and Hilpert, K., Chromium evaporation from SOFC interconnector alloys and degradation process by chromium transport. In *Proceedings of the 1st European Solid Oxide Fuel Cell Forum*, ed. U. Bossel. European Fuel Cell Group, Lucerne, Switzerland, 1994, pp. 703–713.
7. Winkler, W. and Koeppen, J., Design and operation of interconnectors for solid oxide fuel cell stacks. *J. Power Sources,* 1996, **61**, 201–204.
8. Batawi, E., Plas, A., Straub, W., Honegger, K. and Diethelm, R., New cost-effective ceramic oxide phase used as protective coatings for chromium-based interconnects. In *SOFC-VI, PV 99-19*, ed. S. C. Singhal and M. Dokiya. The Electrochemical Society, Pennington, NJ, 1999, pp. 767–773.
9. Hilpert, K., Das, D., Miller, M., Peck, D. H. and Weiβ, R., Chromium vapor species over solid oxide fuel cell interconnect materials and their potential for degradation. *J. Electrochem. Soc.,* 1996, **143**, 3642–3647.
10. Taniguchi, S., Kadowaki, M., Kawamura, H., Yasuo, T., Akiyama, Y., Miyake, Y. and Saitoh, T., Degradation phenomena in the cathode of a solid oxide fuel cell with an alloy separator. *J. Power Sources,* 1995, **55**, 73–79.
11. Badwal, S. P. S., Deller, R., Foger, K., Ramprakash, Y. and Zhang, J. P., Interaction between chromia forming alloy interconnects and air electrodes of solid oxide fuel cells. *Solid State Ionics,* 1997, **99**, 297–310.
12. Jiang, S. P., Zhang, J. P., Apateanu, L. and Foger, K., Deposition of chromium species on Sr-doped $LaMnO_3$ cathodes in solid oxide fuel cells. *Electrochem. Comm.,* 1999, **1**, 394–397.
13. Jiang, S. P., Zhang, J. P., Apateanu, L. and Foger, K., Deposition of chromium species at Sr-doped $LaMnO_3$ electrodes in solid oxide fuel cells. I. Mechanism and kinetics. *J. Electrochem. Soc.,* 2000, **147**, 4013–4022.
14. Jiang, S. P., Zhang, J. P. and Foger, K., Deposition of chromium species at Sr-doped $LaMnO_3$ electrodes in solid oxide fuel cells. II. Effect on O_2 reduction. *J. Electrochem. Soc.,* 2000, **147**, 3195–3205.
15. Jiang, S. P., Zhang, J. P. and Foger, K., Deposition of chromium species at Sr-doped $LaMnO_3$ electrodes in solid oxide fuel cells. III. Effect of air flow. *J. Electrochem. Soc.*, in press.
16. Chen, C. C., Nasrallan, M. M. and Anderson, H. U., Preparation and electrode characteristics of dense $La_{0.6}Sr_{0.4}Co_{0.2}Fe_{0.8}O_3$ thin film by polymeric precursors. In *SOFC-III, PV 93-4*, ed. S. C. Singhal and H. Iwahara. The Electrochemical Society, Pennington, NJ, 1993, pp. 252–266.
17. Winkler, J., Hendriksen, P. V., Bonanos, N. and Mogensen, M., Geometric requirements of solid electrolyte cells with a reference electrode. *J. Electrochem. Soc.,* 1998, **145**, 1184–1192.
18. Jiang, S. P., Love, J. G., Zhang, J. P., Hoang, M., Ramprakash, Y., Hughes, A. E. and Badwal, S. P. S., The electrochemical performance of LSM/zirconia-yttria interface as a function of a-site non-storchiometry and cathodic current treatment. *Solid State Ionics,* 1999, **121**, 1–10.
19. Tsukuda, H. and Yamashita, A., Fundamental research on the change of the microstructure and resistance of solid oxide fuel cells in service. In *Proceedings of the 1st European Solid Oxide Fuel Cell Forum*, ed. U. Bossel. European Fuel Cell Group, Lucerne, Switzerland, 1994, pp. 715–724.
20. Sridhar, S., Stancovski, V. and Pal, U. B., Effect of oxygen-containing species on the impedance of the Pt/YSZ interface. *Solid State Ionics,* 1997, **100**, 17–22.
21. Badwal, S. P. S. and Ciacchi, F. C., Microstructure of Pt electrodes and its influence on the oxygen transfer kinetics. *Solid State Ionics,* 1986, **18/19**, 1054–1060.

22. Carter, S., Selcuk, A., Chater, R. J., Kajda, J., Kilner, J. A. and Steele, B. C. H., Oxygen transport in selected nonstoichiometric perovskite-structure oxides. *Solid State Ionics,* 1992, **53-56**, 597–605.
23. Yasuda, I., Ogasawara, K., Hishinuma, M., Kawada, T. and Dokiya, M., Oxygen tracer diffusion coefficient of (La,Sr)$MnO_{3\delta}$. *Solid State Ionics,* 1996, **86-88**, 1197–1201.
24. Velho, L. R. and Bartlett, R. W., Diffusivity and solubility of oxygen in platinum and Pt–Ni alloys. *Met. Trans.,* 1972, **3**, 65–72.
25. Jiang, S. P., Use of gaseous Cr species to diagnose surface and bulk process for O_2 reduction in solid oxide fuel cells. *J. Appl. Electrochem.,* 2001, **31**, 181–192.
26. Horita, T., Yamaji, K., Sakai, N., Ishikawa, M., Yokokawa, H., Kawada, T. and Kato, T., Active sites imaging for oxygen reduction at the $La_{0.9}Sr_{0.1}MnO_{3-x}$/yttria-stabilized zirconia interface by secondary-ion mass spectrometry. *J. Electrochem. Soc.,* 1998, **145**, 3196–3202.
27. Siebert, E., Hammouche, A. and Kleitz, M., Impedance spectroscopy analysis of $La_{1-x}Sr_xMnO_3$-yttria-stabilized zirconia electrode kinetics. *Electrochim. Acta,* 1995, **40**, 1741–1753.
28. Mizusaki, J., Tagawa, H., Tsuneyoshi, K. and Sawata, A., Reaction kinetics and microstructure of the solid oxide fuel cells air electrode $La_{0.6}Ca_{0.4}MnO_3$/YSZ. *J. Electrochem. Soc.,* 1991, **138**, 1867–1873.
29. Fukunaga, H., Ihara, M., Sakaki, K. and Yamada, K., The relationship between overpotential and the three phase boundary length. *Solid State Ionics,* 1996, **86-88**, 1179–1185.
30. Schwandt, C. and Weppner, W., Kinectics of oxygen, platinum/stabilized zirconia and oxygen, gold/stabilized zirconia electrodes under equilibrium conditions. *Electrochem. Soc.,* 1997, **144**, 3728–3738.
31. Mizusaki, J., Amano, K., Yamauchi, S. and Fueki, K., Electrode reaction at Pt, O_2 (g)/stabalized zirconia interfaces. Part II: electrochemical measurements and analysis. *Solid State Ionics,* 1987, **22**, 323–330.
32. Tai, L. W., Nasrallah, M. M. and Anderson, H. U., $(La_{1-x}Sr_x)(Co_{1-y}Fe_y)O_3$, a potential cathode for intermediate temperature SOFC applications. In *SOFC-III, PV 93-4*, ed. S. C. Singhal and H. Iwahara. The Electrochemical Society, Pennington, NJ, 1993, pp. 241–251.
33. Li, Z., Behruzi, M., Fuerst, L. and Stover, D., Crystalline structure and electrical conductivity of bulk-sintered and plasma-sprayed $La_{1-x}Sr_xMnO_3$ with $0 \leqslant x \leqslant 0.9$. In *SOFC-III, PV 93-4*, ed. S. C. Singhal and H. Iwahara. The Electrochemical Society, Pennington, NJ, 1993, pp. 171–179.
34. Lee, H. Y., Cho, W. S., Oh, S. M., Wiemhöfer, H.-D. and Göpel, W., Active reaction sites for oxygen reduction in $La_{0.9}Sr_{0.1}MnO_3$/YSZ electrodes. *J. Electrochem. Soc.,* 1995, **142**, 2659–2664.
35. Waller, D., Sirman, J. D. and Kilner, J., Manganese diffusion in single crystal and polycrystalline yttria stabilised zirconia. In *SOFC-V, PV 97-40*, ed. U. Stimming, S. C. Singhal, H. Tagawa and W. Lehnert. The Electrochemical Society, Pennington, NJ, 1997, pp. 1140–1149.
36. Benson, S. J., Waller, D. and Kilner, J. A., Degradation of $La_{0.6}Sr_{0.4}Fe_{0.8}Co_{0.2}O_3$ in carbon dioxide and water atmospheres. *J. Electrochem. Soc.,* 1999, **146**, 1305–1309.
37. Miura, N., Okamoto, Y., Tamaki, J., Morinaga, K. and Yamazoe, N., Oxygen semipermeability of mixed-conductive oxide thick-film prepared by slip casting. *Solid State Ionics,* 1995, **79**, 195–200.
38. Jiang, S. P. and Love, J. G., Origin of the initial polarization behavior of Sr-doped $LaMnO_3$ in solid oxide fuel cells. *Solid State Ionics,* 2001, **138**, 183–190.
39. Hou, P. Y., Huang, K. and Bakker, W. T., Promises and problems with metallic interconnects for reduced temperature solid oxide fuel cells. In *SOFC-VI, PV 99-19*, ed. S. C. Singhal and M. Dokiya. The Electrochemical Society, Pennington, NJ, 1999, pp. 737–748.